

# Detecting Differences Between Correlation-Matrix Populations due to Single-variable Perturbations, with Application to Resting State fMRI

Itamar Faran<sup>1</sup>, Michael Peer<sup>2</sup>, Shahar Arzy<sup>3</sup>, and Yuval Benjamini<sup>\*1</sup>

<sup>1</sup>Department of Statistics and Data Science, *Hebrew University of Jerusalem*

<sup>2</sup>Department of Psychology, *University of Pennsylvania*

<sup>3</sup>Department of Medical Neurobiology, *Hebrew University of Jerusalem*

## Abstract

Correlation matrices are widely used to analyze the interdependence of variables in various real-world scenarios. Often, a perturbation in a few variables leads to mild differences in many correlation coefficients associated with these variables. We propose an efficient low-dimensional model that characterizes these differences as a product of single-variable effects. We develop methods for point estimation, confidence intervals, and hypothesis testing for this model. Importantly, our methods can account for both the variability in individual correlation matrices and for within-group variability. In simulations, our model shows increased power compared to competing approaches. We use the model to analyze resting-state functional MRI correlation matrices in patients with transient global amnesia and healthy controls. Our model detects significant decreases in synchronization for the patient population in several brain regions, which could not have been detected using previous methods without prior knowledge. Our methods are available in the open-source package [github.com/itamarfaran/corrpops](https://github.com/itamarfaran/corrpops).

## 1 Introduction

Scientists are often interested in detecting differences in relations between individual variables and the rest of the system, across design conditions. Such differences can occur due to local events affecting one or few variables for some

---

\*Address correspondence to [yuval.benjamini@mail.huji.ac.il](mailto:yuval.benjamini@mail.huji.ac.il)

but not all conditions. These may include the injection of noise to the affected variables, a change in their measurement process, or a breakdown in the synchronization between these variables and the rest of the system. We term these events *single variable perturbation*. Application examples include detecting changes in the relation of particular stocks or markets with respect to the financial portfolio (Longin and Solnik, 1995), detecting distributional differences (*data-drifts*) between train and test sets when porting prediction models (Rabanser et al., 2019), and detecting corrupt sensors (Dunia et al., 1996).

In computational cognitive neuroscience, differences between healthy and patient populations in the temporal synchronization of neural activity across brain regions, measured at rest using functional MRI (RS-fMRI), have been used to characterize neurological diseases and disorders (Biswal et al., 1995). RS-fMRI is a short protocol that can be added to a standard MRI examination, doesn't require any patient cooperation, yet may carry functional information in cases where the disturbance is not apparent structurally; it therefore emerged as a potential source of both neuro-cognitive discoveries and neuro-psychiatric clinical implications. Usually, the sequences are aggregated into correlation coefficients of the BOLD signal (Blood-oxygen-level-dependent) between different brain regions, resulting in person-specific correlation matrices that represent each individual's functional connectivity across brain regions (Lee et al., 2013). In some cases, the differences can be characterized as a reduced association between some brain regions and the rest of the brain (Peer et al., 2014).

We study a two-group design, where  $n_d$  units (or subjects) are observed from the case group ( $\mathcal{D}$ , or disease) and  $n_h$  are observed from the control group ( $\mathcal{H}$  or healthy). For each unit, a  $p$ -dimensional measurement vector is sampled repeatedly ( $T$  times), and these are summarized as a correlation matrix  $R_i \in \mathcal{C}_p$ <sup>1</sup>. The goal of the researcher is to identify and characterize differences between the expected case correlation matrix  $\Lambda^D := E_{i \in \mathcal{D}}[R_i]$  and the expected control correlation matrix  $\Lambda^H := E_{i \in \mathcal{H}}[R_i]$ . Under this formulation, there are  $m := p(p-1)/2$  parameters that can be compared across the two groups. The two-group design is commonly used in RS-fMRI studies: there each unit is an individual, and each  $p$  measurement vector corresponds to the brain activity averaged into  $p$  brain regions over a short ( $\sim 1s$ ) temporal window.  $R_i$  measures the temporal correlations between regions in subject  $i$ .

In the context of correlation matrices, single-variable perturbations manifest as changes in the full rows (and full columns) corresponding to the perturbed variables. These differences would typically be directional: if noise is added to a variable in one condition, or the variable's signal is disturbed, that variable's correlations with all other variables would be smaller in the perturbed condition. Motivated by this principle, we propose a parsimonious model for expressing differences between correlation matrices in terms of individual row-wise (and column-wise) effects.

Methods for detecting differences between correlation matrices have been

---

<sup>1</sup>We use  $\mathcal{C}_p$  for the set of symmetric positive semi-definite  $p \times p$  matrices with a unity diagonal.

studied extensively for the two-samples design (Lawley, 1963; Aitkin et al., 1968; Jennrich, 1970), with recent methods tackling the case where  $T$  is not large compared to the dimension of the matrix  $p$ . Most methods focus either on detecting global differences in the full-matrix (Schott, 2007; Zheng et al., 2019), or on detecting large *local* differences in individual correlation-coefficients (Cai et al., 2013). Additional strategies for dealing with the high-dimension include ridge regularization of the difference matrix or adaptive soft thresholding (Cai and Zhang, 2016). The reader may refer to Cai (2017) and the discussion in Na et al. (2019) for an overview of current methods. However, whereas global tests cannot characterize the nature of the difference, local tests that focus on single-coefficients suffer from low power when the signal is weak and diffuse. Specialized methods can identify weaker signals by focusing on intermediate alternatives such as differences in cliques of variables (Bodwin et al., 2018), on the leading eigenvector of the differential matrix (Zhu et al., 2017), or in sub-networks (Guo and Pagnoni, 2008).

An additional challenge of the two-group design is that each condition is represented by several correlation matrices representing different units. When researchers expect non-negligible differences between units in the group, significant differences are those that exceed this variability. Alas, most statistical methods discussed above do not accommodate this within-group variation. Therefore, researchers in the field turn to standard mass-univariate approaches, calculating a two-group T-statistic for each correlation coefficient (Baker et al., 2014; Brier et al., 2012; Liu et al., 2014; Peer et al., 2014). The resulting p-values or intervals are then corrected to account for multiple comparisons. Because the number of tests grows quadratically with the dimension of the correlation matrix, the corrections for multiplicity reduce the statistical power. This loss of power is considerable when working with small samples, where power is low to begin with<sup>2</sup>. To address this, researchers often artificially reduce the number of regions considered.

In this work, we propose a model attuned to detecting single-variable perturbations that affect the correlation between the groups, while accounting for the variation within the group. Our model describes the difference between groups using a single parameter per variable, allowing efficient comparison between the two groups of correlation matrices:

$$\Lambda^H := E_{i \in \mathcal{H}}[R_i] = \Theta, \quad \Lambda^D := E_{i \in \mathcal{D}}[R_i] = g(\Theta, \alpha), \quad (1.1)$$

for correlation matrix  $\Theta \in \mathcal{C}_p$ ,  $p$ -dimensional parameter vector  $\alpha \in \mathcal{A} \subset R^p$ , and a link function  $g : \mathcal{C}_p \times \mathcal{A} \rightarrow \mathcal{C}_p$ .  $\Theta$  directly models the correlation matrix of the control group, whereas the parameter vector  $\alpha$  specifies a directional change in the correlations for each of the  $p$  variables.  $g$  describes the structure of the divergence between the groups. As our main prototype, we look at the

---

<sup>2</sup>In neuroimaging, collecting larger cohorts has become more common (see the UK Biobank (Sudlow et al., 2015) as an extreme example), but nevertheless smaller samples are still common when researching rare and time-sensitive phenomena, such as in the transient global amnesia example discussed below.

multiplicative link function:

$$g_{jk}(\Theta, \alpha) = \begin{cases} \Theta_{jk} \alpha_j \alpha_k & j \neq k \\ 1 & j = k, \end{cases} \quad (1.2)$$

in which the divergence of the correlation matrices in index  $j, k$  is determined by the interaction of the correlation decay (or growth) of columns-and-rows  $j$  and  $k$ . A finding of  $\alpha_j < 1$  would mean that the correlations of the  $j$  variable with other variables have decayed in the case group, or become smaller in magnitude, compared to those of the control group. Using this parametrization, the dimension of  $\alpha$  (and the number of comparisons) grows *linearly* with the dimension of the correlation matrix, making the model suitable for small sample sizes.

The multiplicative link function incorporates two assumptions on the data. First, the difference between the groups can be summarized into a row-and-column-wise structure. Second, the decay (or increase) in correlations is proportional to the original magnitude of the correlation - originally stronger correlations of the perturbed variables will suffer from greater decay. That is,  $\alpha_j < 1$  represents a decay in correlations for the  $j$ 'th variable, but the magnitude of this decay depends on the correlations in the control group. We find that the vector of decay parameters ( $\alpha$ ) in the multiplicative model can efficiently describe local differences between the groups when the expected correlation matrices are dense.

We propose several strategies to improve the estimation of the parameters and of their uncertainty in the presence of both modeling error and within-group variation. The variables' effects are estimated by finding the roots of an estimation equation that accounts for the asymptotic covariance of correlation matrices (Nel, 1985). We develop robust estimators of the standard deviations using a General Estimating Equations (GEE) framework (Liang and Zeger, 1986), or a less parametric but more computationally intensive two-sample Jackknife procedure (Efron and Stein, 1981). Both of these approaches are designed to measure population variability. Confidence intervals and p-values are based on the approximate Gaussian distribution of GEE solutions.

*Application to Resting-state fMRI Data* We demonstrate our model on RS-fMRI data gathered by Peer et al. (2014) from patients with a unique and rare phenomenon, transient global amnesia (TGA), a phenomenon believed to arise from a perturbation of a single brain region (the Hippocampus) which affects a network of other brain regions. Patients diagnosed with TGA present mainly an acute and complete loss of ability to retain new information (*anterograde amnesia*) and a gradually declining loss of memories to the recent time (*retrograde amnesia*) that resolves autonomously within  $\sim 24$  hours. In recent years, it was discovered that small well-defined lesions may be evident in TGA patients in a certain MRI protocol in a sub-part of the hippocampus, a brain structure that plays a major role in memory processes (Sedlaczek et al., 2004; Bartsch et al., 2006, 2007). Furthermore, an RS-fMRI study recorded within the acute stage revealed a reduction of correlations in hippocampal-related regions (Peer et al., 2014). These disturbances were found at the single-patient level, and their mag-

nitude was correlated to the clinical severity of the impairment. Peer’s study limited the search of connectivity disturbances to the hippocampus in advance, and therefore its findings might have been obscured if no prior hypothesis was assumed. The restricted structural disturbance of TGA and the small sample size (due to TGA rareness) serve as a unique setting to test our model.

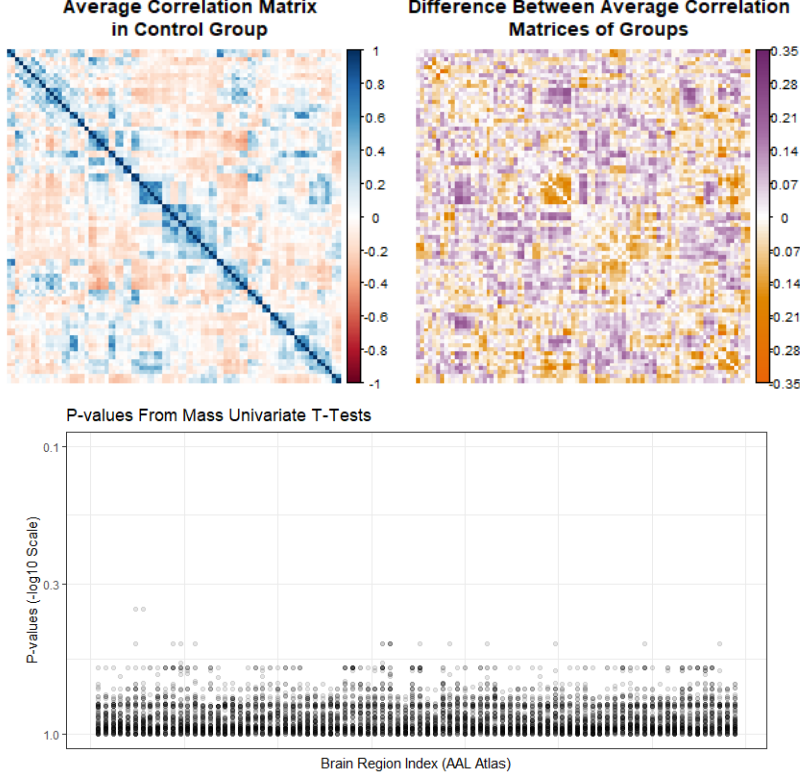


Figure 1: Comparison of the two average correlation matrices from patients with TGA and healthy controls (Peer et al., 2014). Top Left: Average correlation matrix of the control group ( $n_h = 17$ ). Top Right: Differences between average correlation matrices of TGA patients and control subjects. Bottom: Manhattan plot for p-values computed using two-sample t-tests for the correlation coefficients of each region pair (p-value for the correlation of region  $i, j$  appears twice, once in index  $i$  and once in index  $j$ ). p-values are FDR-BH corrected (Benjamini and Hochberg, 1995). The minimal corrected p-value is 0.37. No statistically significant differences would be found without constraints on the search space.

The rest of this paper is organized as follows: In Section 2 we introduce notations and discuss the second moment of correlation matrices, which we will use for our estimation and inferential methods. In Sections 3, 4 we develop an estimator for the parameter-vector of differences between the populations, and

two possible estimators of its variance. In Section 5 we validate and evaluate our model on simulated data in various settings. In Section 6 we apply our methods on RS-fMRI data comparing patients with TGA to controls. Our method finds several significant differences, whereas the mass-univariate analysis finds none. We end with a discussion of potential extensions.

## 2 Notations & Preliminaries

Let  $X_i$  be an observed data matrix of size  $T_i \times p$  measuring  $p$  variables (columns) measured  $T_i$  times (rows) for subject  $i$ . In the fMRI data, the  $p$  columns of  $X_i$  correspond to  $p$  brain regions, sampled at  $T_i$  time points (the rows). We assume that the measurements (rows) of  $X_i$  are centered (mean  $\mathbf{0}$ ), and that  $T_i$  is constant over all subjects ( $T_i = T$ ). For each subject, the measurement matrix  $X_i$  is summarized into the empirical correlation matrix  $R_i$ . Define the empirical covariance operator  $cov(X_i) := T^{-1}X_i^t X_i$ , and the scaling operator on  $W_i = cov(X_i)$  to be  $scale(W_i) := diag(W_i)^{-1/2} \cdot W_i \cdot diag(W_i)^{-1/2}$ . (We use lower-case for matrix operators). The empirical correlation operator on  $X_i$  is  $corr(X_i) := scale(cov(X_i))$ . Finally,  $R_i = corr(X_i)$  is the observed correlation matrix for subject  $i$ . Since correlation matrices are symmetrical, they can be fully characterized using the  $m = \binom{p}{2} = p(p-1)/2$  elements of the upper (or lower) triangle, so we vectorize them in some of the formulas. Define  $vec : \mathbb{M}_p(\mathbb{R}) \mapsto \mathbb{R}^m$  as the vectorization operator with  $vec(R) := (R_{12}, R_{13}, \dots, R_{1p}, R_{23}, \dots, R_{p-1,p})^t$ , or alternatively  $\vec{R} := vec(R)$ . We use the  $\circ$  notation to denote the Hadamard product between matrices;  $E[\cdot]$  and upper-case  $Cov(\cdot)$  to denote the first and second moments of random vectors or matrices. We denote the  $p$ -dimensional multivariate Gaussian distribution by  $\mathcal{N}_p(\boldsymbol{\mu}, \Sigma)$  and its PDF by  $\phi_p(x, \boldsymbol{\mu}, \Sigma)$ . Finally, we denote the Matrix-Gaussian distribution with  $Y \sim \mathcal{MN}_{T \times p}(\mathbf{M}, \Delta, \Sigma)$ , remembering that for rows  $Y_{t.} \sim \mathcal{N}_p(\mathbf{M}_{t.}, \Delta_{tt} \cdot \Sigma)$ , and for columns  $Y_{.j} \sim \mathcal{N}_T(\mathbf{M}_{.j}, \Delta \cdot \Sigma_{jj})$ .

### Moments of Empirical Correlation Matrices

Here we review the moments of correlation matrices estimated from correlated Gaussian vectors (for general results see Neudecker and Wesselman (1990) and Schott (2005); for the effect of temporal correlation on inference see Afyouni et al. (2019) and Efron (2008, 2012)). We use these results in estimating our model below. Readers may choose to skip directly to Section 3.

Let  $X$  be a random data matrix of size  $T \times p$ , and assume that  $X \sim \mathcal{MN}_{T \times p}(\mathbf{0}, \Delta, \Sigma)$ . When the rows are *i.i.d* ( $\Delta = I_T$ ),  $W = cov(X)$  is the maximum likelihood estimator for  $\Sigma$ , and  $T \cdot W$  follows a *Wishart* $_p(\Sigma, T)$  distribution. The first two moments of  $W$  are then given by:

$$E[W] = \Sigma, \quad (2.1)$$

$$T \cdot Cov(W_{ij}, W_{kl}) = \Sigma_{ij,kl}^{(2)} = \Sigma_{ik}\Sigma_{jl} + \Sigma_{il}\Sigma_{jk}, \quad (2.2)$$

as shown for example in Efron (2012). However, the elements of the empirical correlation matrix have distinctly smaller variances due to the scaling. The following lemma describes the limiting covariance of values in the empirical correlation matrix:

**Lemma 1.** *The asymptotic moments of the empirical correlation matrix for i.i.d samples. Let  $R = \text{corr}(X)$  for  $X \sim \mathcal{MN}_{T \times p}(\mathbf{0}, I_T, \Sigma)$ . Denote by  $\boldsymbol{\rho} = \text{scale}(\Sigma)$ , or  $\rho_{ij} = \Sigma_{ij} / \sqrt{\Sigma_{ii}\Sigma_{jj}}$ . Then  $\lim_{T \rightarrow \infty} E[R] = \boldsymbol{\rho}$ , and  $\lim_{T \rightarrow \infty} T \cdot \text{Cov}(R_{ij}, R_{kl}) = C_{ij,kl}(\boldsymbol{\rho})$ , where*

$$C_{ij,kl}(\boldsymbol{\rho}) := \frac{\rho_{ij}\rho_{kl}}{2} (\rho_{ik}^2 + \rho_{il}^2 + \rho_{jk}^2 + \rho_{jl}^2) - \rho_{ij}(\rho_{ik}\rho_{il} + \rho_{jk}\rho_{jl}) \quad (2.3)$$

$$- \rho_{kl}(\rho_{ik} \cdot \rho_{jk} + \rho_{il} \cdot \rho_{jl}) + (\rho_{ik}\rho_{jl} + \rho_{il}\rho_{jk}).$$

The lemma was introduced by Pearson and Filon (1898) and is listed by Nel (1985) and Schott (2005), and is derived using a first-order approximation of the  $\text{corr}(\cdot)$  function on the empirical covariance matrix. The convergence is of the moments of  $R$ , in that higher order terms vanish as sample size increases. Finally, we can turn the element-wise operations in (2.3) into a matrix operator  $C : \mathcal{C}_p \rightarrow M_m(R)$ :

$$C(\vec{\rho}) \doteq T \cdot \text{Cov}(\vec{R}). \quad (2.4)$$

Later, we will plugin the observed correlation matrices  $R_i$  into the operator  $C$ .

### Accounting for Temporal Correlation

In fMRI time-series data (or other data characterized by temporal correlation), the correlation between adjacent rows can be large, and hence less information is added from each row compared to the i.i.d case. While  $W$  remains an unbiased estimator of  $\Sigma$ , the covariance of  $W$  and  $R$  will be larger than the expression in (2.3). The following correction, due to Efron (2012), identifies an effective degrees of freedom  $T_{eff}$ , which can be estimated directly from  $\Sigma$ . We cite the result with no proof.

**Lemma 2.** *The asymptotic moments of empirical correlation matrices for correlated samples. Let  $X \sim \mathcal{MN}_{T \times p}(\mathbf{0}, \Delta, \Sigma)$  for a general positive-definite  $\Delta$ , and let  $W = \text{cov}(X)$  and  $R = \text{corr}(X)$ . Define  $\psi(\Sigma)$  to be the root-mean-square correlation:  $\psi = m^{-1} \sum_{i < j} \rho_{ij}^2$ . Then the covariance of the correlation matrix shrinks like the effective degrees of freedom  $T_{eff}(T, \psi) = T / (1 + (T - 1) \cdot \psi^2)$ , namely*

$$T_{eff}(T, \psi) \cdot \text{Cov}(W_{ij}, W_{kl}) = \Sigma_{ij,kl}^{(2)}, \quad \lim_{T_{eff} \rightarrow \infty} T_{eff}(T, \psi) \cdot \text{Cov}(R_{ij}, R_{kl}) = C_{ij,kl}(\boldsymbol{\rho}).$$

To summarize the above lemmas, the first two moments of the vectorized empirical correlation matrix  $\vec{R}$  can be described

$$E[\vec{R}] \xrightarrow{T_{eff} \rightarrow \infty} \vec{\rho}, \quad \text{Cov}[\sqrt{T_{eff}} \cdot (\vec{R} - \vec{\rho})] \xrightarrow{T_{eff} \rightarrow \infty} C(\boldsymbol{\rho}). \quad (2.5)$$

### 3 A Model for Differences Between Correlation Matrices

The data consists of correlation matrices  $\{R_1, R_2, \dots, R_{n_d+n_h}\} \subset \mathcal{C}_p$ , with  $i \in \mathcal{H}$  representing samples from the control group and  $i \in \mathcal{D}$  samples from the case group. Setting together (1.1), we can describe the matrices using the following additive model:

$$R_i = \begin{cases} \Theta + \epsilon_i & i \in \mathcal{H}, \\ g(\Theta, \alpha) + \epsilon_i & i \in \mathcal{D}. \end{cases} \quad E[\epsilon_i] = \mathbf{0}. \quad (3.1)$$

$\epsilon_i$ 's are symmetric matrices with zeroed diagonals, representing the joint residuals due to (a) the noise in estimating each correlation matrix, (b) the variation across units within the groups, and (c) the modeling error of the group mean. Note that the modeling error in (c) comes from the restrictive parameterization of the group means using  $\Theta$  and  $g(\Theta, \alpha)$ . This modeling error vanishes if the two group means are identical (that is, under the global null).

For the model to be useful, we need to identify link functions  $g$  and corresponding parameter sets  $(\Theta, A(\Theta)) \subset \mathcal{C}_p \times \mathcal{A}$  where the model behaves well. We look for the following properties:

1. **Resulting with a correlation matrix:** For any  $(\Theta, \alpha) \in (\Theta, A(\Theta))$ ,  $g(\Theta, \alpha)$  is a member of  $\mathcal{C}_p$ , meaning a symmetric and positive semi-definite matrix with a unity diagonal.
2. **Identifiable:** The model in (3.1) is identifiable.
3. **Invertible by  $\alpha$ :** There exists  $g^{-1}(g(\Theta, \alpha), \alpha) = \Theta$ .
4. **Continuously differentiable:** The derivatives  $\frac{\partial g_j}{\partial \alpha_k}$  are defined and continuous.

Properties 1 and 2 are required for the parametrization in (3.1), and Properties 3 and 4 are used for the estimation algorithm we propose. Whereas the rest of this paper treats the link function abstractly, next we discuss our prototype link.

#### The Multiplicative Link Function

The multiplicative link (1.2) is our prototype for  $g$  throughout this paper. The multiplicative link function can be presented in matrix form as  $g(\Theta, \alpha) = \Theta \circ \alpha \alpha^t + I - D_\alpha^2$ , where  $D_\alpha$  is a diagonal matrix with entries  $[D_\alpha]_{ii} = \alpha_i$  and 0 otherwise. The multiplicative link is useful to model changes between the groups when the original correlation matrix is relatively dense. This link function incorporates two assumptions regarding the directions of change between populations:



- *Assumption 1:* Researchers are interested in identifying variables where the correlation profile has changed directionally between two populations (increased or reduced correlation).
- *Assumption 2:* The expected magnitude of the difference between correlation coefficients would be proportional to the magnitude of the original correlation.

We expect most  $\alpha_j$ 's to be near 1, where  $\alpha_j = 1$  indicates no directional change.

With respect to TGA, we may ask if there is a perturbation in the patient group that leads to reduced connectivity between one brain region and its neighbors compared to the healthy group. In that case, we would expect the correlations involving that region to decay toward 0. We would further expect the strongest decay (in absolute terms) to be in pairs originally showing the strongest correlations. In our model, these effects would be represented by having  $\alpha_j < 1$ . The model with multiplicative link meets the requirements under the following conditions:

1. **Resulting with a correlation matrix:** Let  $\lambda_p$  be the minimal eigenvalue of  $\Theta$ , and  $\alpha_m, \alpha_M$  are the maximal and minimal values of  $|\alpha_j|$ , respectively. Then a sufficient condition for  $g(\Theta, \alpha) \in \mathcal{C}_p$  is that  $\lambda_p \cdot \alpha_m^2 \geq \alpha_M^2 - 1$ . The model is therefore well defined for  $\alpha_M \leq 1$ , and, in the typical case where  $\lambda_p, \alpha_m > 0$ , for  $\alpha_M$  in the neighborhood around 1. The proof is given in the Appendix A.1.
2. **Identifiable:** The multiplicative link model is identifiable if  $\vec{\Theta}$  has a sufficiently many non-zero entries. Concretely, define  $e^{(j)}$  the elementary vectors of size  $p$ ,  $e^{(j,k)} = e^{(j)} + e^{(k)}$ , and  $\tilde{m}$  the number of non-zero entries in  $\vec{\Theta}$ . Let  $A$  be the matrix of dimension  $\tilde{m} \times p$  with  $e^{(j,k)}$  in it's rows, corresponding to  $\vec{\Theta}$ 's non-zero entries. Then, assuming  $\alpha_j > 0$  for all  $j$ , the model (3.1) with the multiplicative link is identifiable if  $\text{rank}(A) = p$ . The proof and the conditions for the case where  $\alpha_j \geq 0$  are given in the Appendix A.2.
3. **Invertible by  $\alpha$ :** If  $\alpha_j \neq 0$  for all  $j$ , the multiplicative link function's inverse can be expressed as  $g_{jk}^{-1}(\Theta, \alpha) = \frac{\Theta_{jk}}{\alpha_j \alpha_k}$  for  $j \neq k$ , and 1 otherwise.
4. **Continuously differentiable:** The multiplicative link function is differentiable for any  $\alpha_j$ :  $\frac{\partial g_{jk}}{\partial \alpha_k} = \Theta_{ij} \alpha_i$  for  $k = j \neq i$ , and 1 otherwise.

We can conclude that for  $\alpha$  values separated from 0, and a sufficiently dense correlation matrix  $\Theta$ , the model is well formed. We find these conditions to hold well empirically for RS-fMRI datasets.

#### **Remark**

The model can be seen as an adaptation of two-way models for table data to correlation matrices. To see this, consider the following two-way model for two groups of  $p \times p$  data tables, where the effect of the case group is composed of separate additive or multiplicative row effects  $\tau$  and column effects  $\nu$ :

$E_{i \in \mathcal{H}}[Y_{jk}^i] = \mu_{jk}^H$ , and  $E_{i \in \mathcal{D}}[Y_{jk}^i] = \mu_{jk}^H \cdot \tau_j \cdot \nu_k$ . When we adapt this to correlation matrices, the symmetry means that row and column effects are the same, resulting in our model above.

## 4 Model Estimation

Our target of estimation is the parameter vector of differences  $\alpha$ , whereas we treat  $\Theta$  as a nuisance parameter. We assume that each (vectorized) correlation matrix is approximately Gaussian distributed (see Hlinka et al. (2011) and Adrian et al. (2013) for a discussion on the validity of this approximation in RS-fMRI). The sampling covariance of correlation matrices depends on their mean through operator  $C(\cdot)$ , as developed in (2.5). One approach for estimation is to apply the mean model (1.1) for the covariance estimation, using  $Cov(\vec{R}_i)$  with  $C_\Theta = C(\Theta)$  for the control examples and  $C_g = C(g(\Theta, \alpha))$  for the cases. This would result in a full log-likelihood function:  $\ell \propto \sum_{i \in \mathcal{H}} \ln \phi_m(\vec{R}_i, \vec{\Theta}, C_\Theta) + \sum_{i \in \mathcal{D}} \ln \phi_m(\vec{R}_i, \vec{g}(\Theta, \alpha), C_g)$ . However, tying the covariance term to the free parameters of the model increases the burden on the optimization procedure, as updating the covariance of the correlation matrices is hard. Furthermore, this formulation is less robust to deviations from the model's assumptions regarding the link function  $g$  and to the choice of the optimization algorithm.

We therefore turn to a general least squares formulation where the covariance matrix does not change with  $\alpha$  nor  $\Theta$ . Instead, we define  $\bar{C}_d = n_d^{-1} \sum_{i \in \mathcal{D}} C(R_i)$ , and similarly  $\bar{C}_h = n_h^{-1} \sum_{i \in \mathcal{H}} C(R_i)$ , and use these as weighting matrices in the quadratic loss function  $\mathcal{S}(\Theta, \alpha) = \mathcal{S}^h(\Theta) + \mathcal{S}^d(\Theta, \alpha)$ , where

$$\begin{aligned} \mathcal{S}^h(\Theta) &= \sum_{i \in \mathcal{H}} \left( \vec{R}_i - \vec{\Theta} \right)^t \bar{C}_h^{-1} \left( \vec{R}_i - \vec{\Theta} \right), \\ \mathcal{S}^d(\Theta, \alpha) &= \sum_{i \in \mathcal{D}} \left( \vec{R}_i - \vec{g}(\Theta, \alpha) \right)^t \bar{C}_d^{-1} \left( \vec{R}_i - \vec{g}(\Theta, \alpha) \right). \end{aligned}$$

Our estimators are defined as  $\hat{\Theta}, \hat{\alpha} = \arg \min_{\Theta, \alpha} \mathcal{S}$ . This optimization does not depend on the determinant of  $C_g$  and therefore yields more stable results than the model in (4).

For intermediate dimension  $p$ , optimizing the loss function  $\mathcal{S}$  on  $\Theta$  and  $\alpha$  jointly is still computationally expensive due to the large model space. We optimize the parameters in an alternating manner: at each step we optimize on  $\alpha$  by gradient descent, and reestimate  $\Theta$  by inverting the method-of-moments estimator. Formally, let  $\hat{\Theta}_{k-1}$  be our estimate of  $\Theta$  at the  $k-1$  step, then the

updates for  $\hat{\alpha}_k, \hat{\Theta}_k$  at step  $k$  are given by:

$$\hat{\alpha}_k = \arg \min_{\alpha} \mathcal{S}^d \left( \hat{\Theta}_{k-1}, \alpha \right), \quad (4.1)$$

$$\hat{\Theta}_k = (n_h + n_d)^{-1} \left( \sum_{i \in \mathcal{H}} R_i + \sum_{i \in \mathcal{D}} g^{-1} (R_i, \hat{\alpha}_k) \right). \quad (4.2)$$

As initial values for the optimization, we set  $\hat{\alpha}_0$  in Equation 4.1 to its null-value indicating  $\Lambda^H = \Lambda^D$ . For the multiplicative link function, this is  $\hat{\alpha}_0 = \mathbf{1}$ .

#### 4.1 Model Inference

The estimation of  $\alpha$  is viewed as a solution of a set of estimation equations: for a non-boundary minima of  $\mathcal{S}$  by  $\alpha$ , the estimation error will be approximately Gaussian:

$(n_h^{-1} + n_d^{-1})^{-1/2} \cdot (\hat{\alpha} - \alpha) \sim \mathcal{N}_p(\mathbf{0}, V(\hat{\alpha}))$ , where  $V(\hat{\alpha})$  is the covariance matrix of our estimates. We propose two methods for estimating  $V(\hat{\alpha})$ : the sandwich

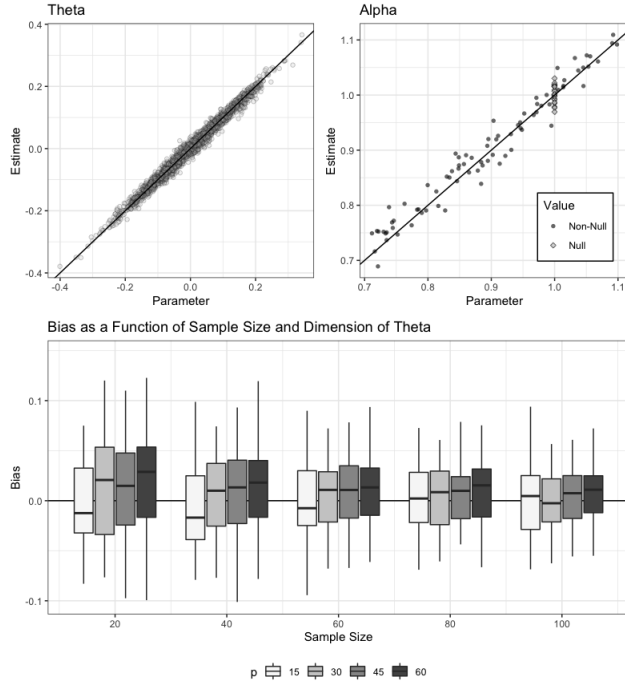


Figure 2: Estimation results. Top: Comparison of estimates and parameters in a single simulation. Bottom: Boxplot of the bias  $\hat{\alpha} - \alpha$  as a function of sample size  $n$  (x-axis) and dimension  $p$  (shade). Each boxplot consists of  $p \cdot B$  values of  $\alpha$  where  $B = 3$  simulation repetitions.

estimator based on the Generalized Estimation Equations (GEE) framework (Liang and Zeger, 1986); and a two-sample Jackknife procedure that requires less assumptions but larger sample sizes and more computation.

#### 4.1.1 GEE Estimate of $V(\hat{\alpha})$

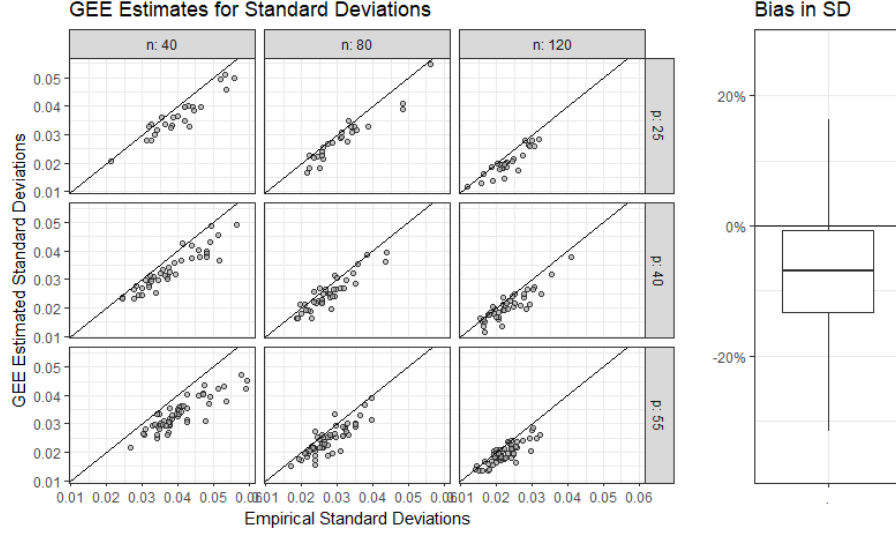


Figure 3: SD estimation with GEE. Left: Estimated standard deviation ( $SD(\hat{\alpha})$ , via GEE) versus true values (via empirical parametric bootstrap) for various  $n, p$  values. Simulations were conducted under the weak null and with positive auto-correlation. Right: Boxplot showing the percentage bias  $\sqrt{\hat{V}(\hat{\alpha}_j)} / \text{Var}(\hat{\alpha}_j) - 1$  from all simulations.

$V(\hat{\alpha})$  can be estimated with a sandwich estimator, following Liang and Zeger (1986):  $\hat{V}_{gee}(\hat{\alpha}) = I^{(0)-1} I^{(1)} I^{(0)-1}$  where  $I^{(0)} = I_h^{(0)} + I_d^{(0)}$  and  $I^{(1)} = I_h^{(1)} + I_d^{(1)}$ . These, in turn, are defined as:

$$I_d^{(0)} = n_d \cdot \mathbf{J}_\alpha g^t \cdot \bar{C}_d^{-1} \cdot \mathbf{J}_\alpha g|_{\alpha=\hat{\alpha}}, \quad I_d^{(1)} = n_d \cdot \mathbf{J}_\alpha g^t \cdot \bar{C}_d^{-1} \cdot \Upsilon_d \cdot \bar{C}_d^{-1} \cdot \mathbf{J}_\alpha g|_{\alpha=\hat{\alpha}} \quad (4.3)$$

$$I_h^{(0)} = n_h \cdot \mathbf{J}_\alpha \hat{\Theta}^t \cdot \bar{C}_h^{-1} \cdot \mathbf{J}_\alpha \hat{\Theta}|_{\alpha=\hat{\alpha}} \quad I_h^{(1)} = n_h \cdot \mathbf{J}_\alpha \hat{\Theta}^t \cdot \bar{C}_h^{-1} \cdot \Upsilon_h \cdot \bar{C}_h^{-1} \cdot \mathbf{J}_\alpha \hat{\Theta}|_{\alpha=\hat{\alpha}} \quad (4.4)$$

where  $\mathbf{J}_\alpha g$  is the Jacobian matrix of  $\vec{g}(\hat{\Theta}, \alpha)$  by  $\alpha$  ( $[\mathbf{J}_\alpha g]_{ij} = \frac{\partial \vec{g}_i(\hat{\Theta}, \alpha)}{\partial \alpha_j}$ ),  $\mathbf{J}_\alpha \hat{\Theta}$  is the Jacobian matrix of  $\hat{\Theta}$  by  $\alpha$ , and  $\Upsilon_d$  is an empirical estimate of the covariance of  $\vec{R}_i$  (for  $i \in \mathcal{D}$ ):

$$\Upsilon_d = (n_d - 1)^{-1} \sum_{i \in \mathcal{D}} \left( \vec{R}_i - \vec{g}(\hat{\Theta}, \hat{\alpha}) \right) \left( \vec{R}_i - \vec{g}(\hat{\Theta}, \hat{\alpha}) \right)^t.$$

$\Upsilon_h$  is defined similarly. Note that in theory,  $\bar{C}_d$  should be divided by  $T_{eff}$  in equations (4.3),(4.4); in practice  $T_{eff}$  cancels out in the multiplication of  $V(\hat{\alpha})$ , and so it is omitted.

#### 4.1.2 Jackknife Estimate of $V(\hat{\alpha})$

Alternatively, we propose a non-parametric method of estimating  $V(\hat{\alpha})$  with a Jackknife procedure (Efron and Stein, 1981). This framework can be used in cases where the GEE framework underestimates the variance, for example when the proportion of the control group is small (Figure 6). Here, each subject is omitted in turn from the sample, and  $\alpha$  is re-estimated. Call  $\hat{\alpha}_{(-i)}$  the estimate calculated when omitting subject  $i$ , and call  $\hat{\alpha}_d = n_d^{-1} \sum_{i \in \mathcal{D}} \hat{\alpha}_{(-i)}$  ( $\hat{\alpha}_h$  defined similarly). Then the Jackknife estimate is defined as  $\hat{\alpha}_{jack} = \frac{n_h \cdot \hat{\alpha}_h + n_d \cdot \hat{\alpha}_d}{n_h + n_d}$ . The variance of the Jackknife estimate is estimated with  $\hat{V}_{jack}(\hat{\alpha}) = \nu_d + \nu_h$  where  $\nu_d = \frac{n_d - 1}{n_d} \sum_{i \in \mathcal{D}} (\hat{\alpha}_{(-i)} - \hat{\alpha}_d) \cdot (\hat{\alpha}_{(-i)} - \hat{\alpha}_d)^t$  and  $\nu_h$  is defined similarly. In practice, we use a warm start for  $\hat{\alpha}_{(-i)}$  for faster convergence.

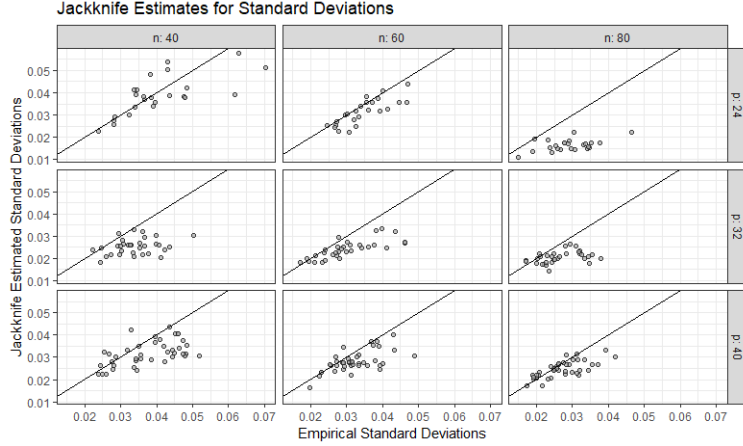


Figure 4: SD estimation with Jackknife. Estimated standard deviation versus true values for various  $n, p$  values. Simulations were conducted under the weak null and with positive auto-correlation.

#### 4.1.3 Inference on $\alpha$ and Accounting for Multiplicity

After estimating  $V(\hat{\alpha})$ , we can assume that the estimators derived in Section 4 have a limiting distribution of  $\hat{V}(\hat{\alpha})^{-1/2}(\hat{\alpha} - \alpha) \sim \mathcal{N}_p(0, I_p)$ , and calculate the Z-values, p-values, and confidence intervals accordingly. We correct the p-values and confidence intervals to keep the FDR and FCR accordingly using the BH procedure (Benjamini and Hochberg, 1995; Benjamini and Yekutieli, 2005).

## 5 Simulations

In this section, we validate and evaluate the model on simulated data. The data is simulated in accordance to the model’s assumptions with the multiplicative link function. In each experiment, we randomly generate a dense spatial covariance matrix  $\Theta$ . For each subject, we generate  $T$  multivariate Gaussian measurements with  $\Theta$  covariance for the control subjects and  $g(\Theta, \alpha)$  for patient subjects. From these measurements, we compute the sample correlation matrix for each subject. The measurements are simulated either from a multivariate  $ARMA(1, 1)$  process with both AR and MA parameters equal to .5 to approximate the temporal correlation expected in RS-fMRI scans (Luo et al., 2020; Locascio et al., 1997), or with temporal-independence as a benchmark. More details about the simulations are in the appendix (Section D).

### 5.0.1 Validation of the Inferential Methods

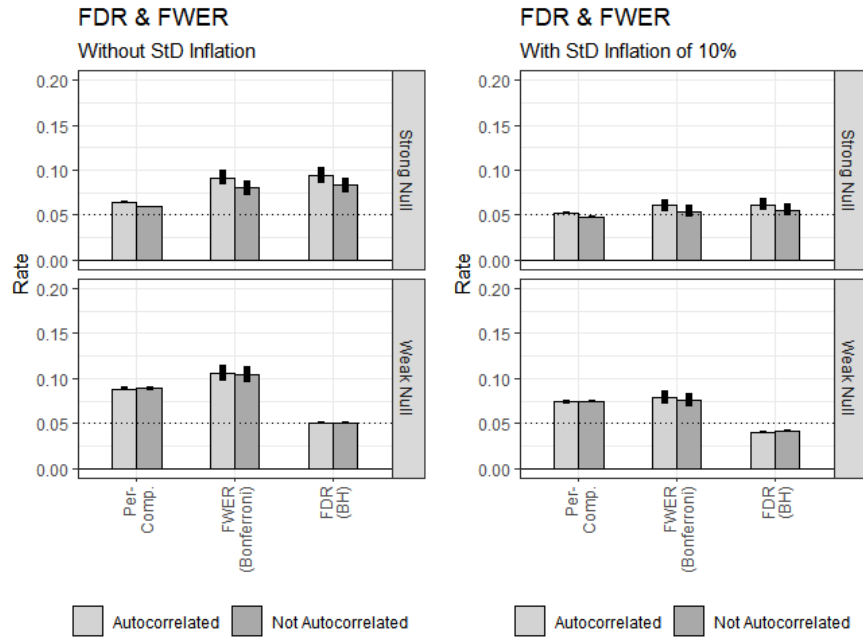


Figure 5: Error rates for testing partial hypotheses  $\{H_{(0),j} : \alpha_j = 1\}$  under the weak and strong null. We plot the per-comparison error rate, family-wise error rate (FWER) after Bonferroni correction, and false discovery rate (FDR) after BH correction. p-values are based on  $\hat{V}_{gee}$  estimates of variance, with and without the standard deviation inflation of 10%. Bars indicate a  $\pm 1$  SD range. Data were simulated with  $n_h = n_d = 50$  and  $p = 32$ .

In Figure (2), we compare the estimates to the parameters of the model and inspect the bias of  $\alpha$ 's estimates. In the top panel, we set  $n = 100$  and  $p = 50$ , with 10 of the  $\alpha_j$ -s equal to 1 and the rest vary between  $[0.7, 1.1]$ . In the bottom panel, we allow the sample size and the dimension  $p$  to vary with 3 replications. The results suggest that both the bias and spread of  $\hat{\alpha}$  decrease as the sample size increases.

Next, we compare the GEE framework estimators of variance to the observed variance. We use a parametric bootstrap procedure: for each randomly generated set of  $\Theta, \alpha$  we simulated 100 datasets and estimated the empirical variance of  $\hat{\alpha}$  across datasets. We compared this result to the average GEE variance estimate over all datasets. In Figure (3) we hold the proportion of the patient group size  $n_d/(n_d + n_h)$  constant at .5, and allow  $n$  and  $p$  to vary. The  $\alpha$ 's are not fixed at 1, and a positive temporal correlation is introduced. In Figure (4) we repeat the experiment but this time estimate the variation using the Jackknife framework. Both figures suggest that the estimated standard deviations characterize well the true deviation of the  $\hat{\alpha}$ s values. In Figure (6), we varied the proportion of the patient group size  $n_d/(n_d + n_h)$  and examined its effect on the bias of the GEE variance estimator. Each boxplot represents a different imbalance. We find that the GEE variance estimators are sensitive to a severe imbalance between group sizes.

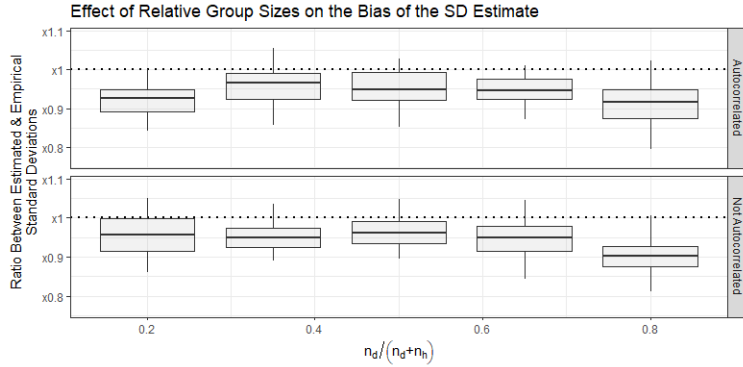


Figure 6: Effect of the relative size of the patient group ( $\frac{n_d}{n_h + n_d}$ ) on the SD estimator (GEE). Strong imbalance between the sizes of the groups increases the bias of  $\sqrt{\hat{V}_{gee}}$ . In all runs,  $n = 50$  and  $p = 25$

Importantly, Figures (3) and (6) indicate that the GEE variance estimators slightly underestimate the variance. To account for this issue, we inflate standard deviations produced by this framework by 10% as a heuristic. We conducted this inflation in the following simulations and in the analysis of the TGA data in Section 6 as well.

Figure (5) examines the control of the FWER (with Bonferroni's correction) and the control of the FDR (using BH correction) under four situations: under

the strong null (all null hypotheses are true) and the weak null (some alternative hypotheses are true), and when temporal correlations are or are not present. The results are shown without (left) and with inflating the standard deviations.

### 5.0.2 Comparing Power of Different Approaches

Figure (7) compares the statistical power of our method to the mass-univariate approach. For each correlation coefficient  $(k, l)$ , we conduct a T-test comparing the means of  $\{\zeta(R_{i,kl})\}_{i \in \mathcal{D}}$  to  $\{\zeta(R_{i,kl})\}_{i \in \mathcal{H}}$  where  $\zeta$  is Fisher's Z-Transformation (Fisher, 1921). We correct the p-values using the BH procedure and compare the proportion of rejections on voxels having  $\{k, l : \Lambda_{kl}^H \neq \Lambda_{kl}^D\}$ , to the proportion of columns rejected having  $\alpha \neq 1$ . We find that our method detects more variables with non-null effects compared to the mass-univariate approach. When the number of columns affected increases, the proportion of rejections in our model is reduced (top left figure). We hypothesize that as more columns are affected, it is harder for the model to identify the columns.

In Figure (8) we compare our method to the sparse leading eigenvalue (sLED) method of Zhu et al. (2017). sLED formulates a permutation test for testing whether the correlation matrices for two groups of independent vectors are identical. For the test statistic, it finds the leading sparse eigenvalue of the difference between correlations. We modified their permutation test to match the structure of multi-subject data, permuting the assignment of the correlation matrices into the groups. Although their test benefits from the sparsity of the leading eigenvector, it can only infer for the full vector, not for differences in individual

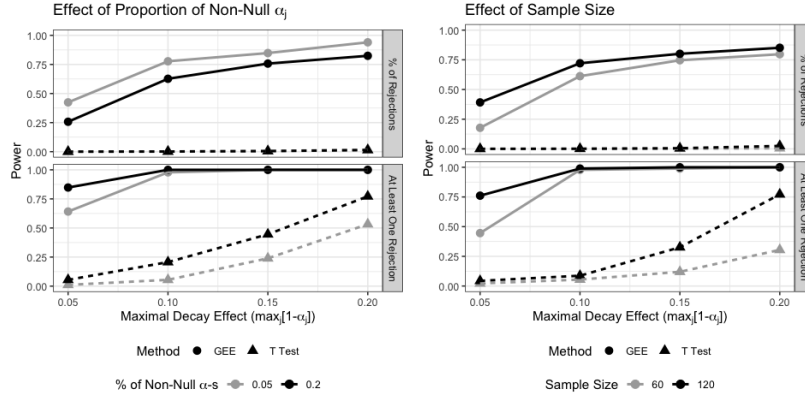


Figure 7: Comparison of power between our method (●, solid line) and the mass-univariate approach (▲, dashed line). On the x-axis, the effect size  $(1 - \max_j \alpha_j)$ . On the top panel, power is defined as the probability to reject the global null. On the bottom, it is defined as the proportion of rejected non-null  $\alpha_j$ -s. On the left, the sample size is held constant ( $n = 100$ ) and the % of non-null  $\alpha_j$ -s vary by color. On the right, the percent of non-null  $\alpha_j$ -s is held constant (10%) and the sample size varies by color.



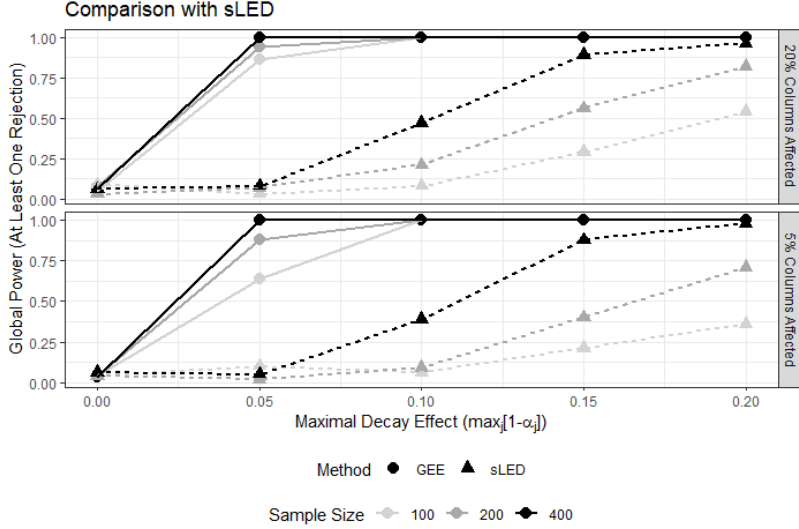


Figure 8: Comparison of power between our method (●, solid line) and the sLED method of Zhu et al. (2017) (▲, dashed line). On the x-axis, the effect size ( $1 - \max_j \alpha_j$ ). On the y-axis, the probability to reject the global null. Sample size varies by color.

coordinates of the vector. Therefore, we define the power for our method as the probability of rejecting the null for at least one variable (after multiplicity corrections), and compare this to the probability of rejecting the global null under the sLED method. We find a substantial increase in the power of our method to reject the global null compared to sLED for multiple effect sizes and sample sizes.

In Supplementary Figure (12) we examine the computation time as a function of  $p$ ; we find calculation time scales as  $m^{2.3}$ , the time complexity of the inversion of  $\tilde{C}_d$  (an  $m \times m$  matrix).

## 6 Application on Data From Patients with TGA

We refer to the RS-fMRI data recorded by Peer et al. (2014) from patients with acute transient global amnesia (TGA) to demonstrate our proposed model. In the original paper, the data was analyzed using the mass-univariate approach. In order to preserve statistical power, the authors focused their investigation to suspected brain regions and they grouped together activity across known sets of brain regions to limit the number of comparisons. While these practices could detect statistically significant differences between the groups, they limited the ability to detect differences in brain regions that the researchers had no prior hypothesis on. In contrast, our model finds statistically significant decays in the correlations of several hippocampal and adjacent temporal lobe regions without

using prior information to limit the search.

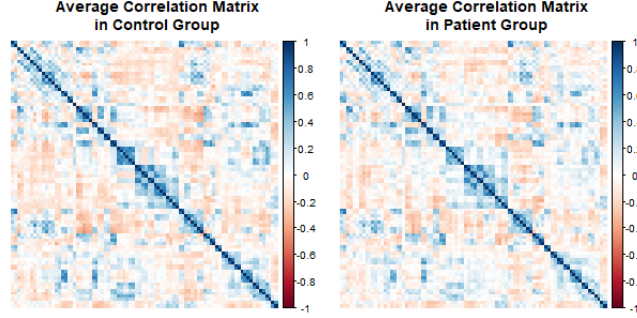


Figure 9: The average correlation matrices of control subjects (left) and TGA patients (right).

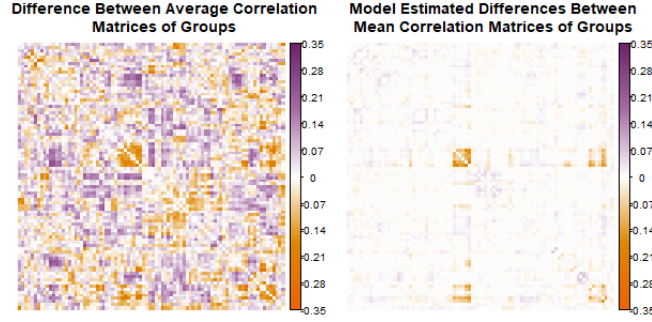


Figure 10: Left: Observed differences between TGA patients and control subjects ( $\bar{R}_d - \bar{R}_h$ ). Right: Model estimated differences ( $\hat{\Theta}_{ij}\hat{\alpha}_i\hat{\alpha}_j - \hat{\Theta}_{ij} = \hat{\Theta}_{ij}(\hat{\alpha}_i\hat{\alpha}_j - 1)$ )

The data consists of  $n_d = 12$  patients (aged  $62.7 \pm 7.4$ ; 5 male) that met the standard clinical criteria for a diagnosis of TGA, matched by  $n_h = 17$  volunteers (aged  $62.1 \pm 6.9$ ; 8 male) that serve as the control group. Patients were scanned with functional MRI during the few hours of the acute amnesic state. The rarity of TGA and the time constraints explain the small sample sizes in this study. We refer the reader to the original paper for details on the fMRI processing and extraction of activity patterns in each region. The whole brain network was defined according to the Automatic Anatomical Labeling (AAL) atlas, which defines 45 brain regions in each cerebral hemisphere (Tzourio-Mazoyer et al., 2002). 4 regions were omitted from the analysis as some subjects had missing values in the corresponding columns, resulting in correlation matrices of dimension  $p = 86$ . In Figure (9) we display the average correlation matrix of each group.

When analyzing the data using the multiplicative link, we found an upwards bias in the estimates:  $\hat{\alpha}_j$  tends to be consistently higher than 1, possibly due to the preprocessing. To remove this bias we conduct a location correction:

$\tilde{\alpha} = \hat{\alpha} - M(\hat{\alpha}) + 1$ , with  $M(\cdot)$  representing the median operator and 1 is added since it is the null value of the multiplicative link function. We estimated  $V(\hat{\alpha})$  using the GEE method, and inflated the standard deviations by 10%. The p-values and intervals were corrected to keep the FDR and FCR respectively (Benjamini and Yekutieli, 2005).

Table 1: Regions with statistically significant decay (FCR & FDR corrected)

AAL Index	Region	$\tilde{\alpha}_j$ (CI, FCR Adj.)	P-value FDR-Adj.
37	Hippocampus (L)	0.907 (0.84 - 0.97)	.005
41	Amygdala (L)	0.848 (0.76 - 0.94)	.002
42	Amygdala (R)	0.784 (0.69 - 0.88)	<.0001
83	Temporal Pole (L)	0.913 (0.85 - 0.98)	.0087
87	Temporal Pole (L)	0.842 (0.74 - 0.97)	.005

In Figure (10) we show the observed difference ( $\bar{R}_d - \bar{R}_h$ ) and the estimated difference through the link function. Our methodology underestimates the differences in comparison to the mass univariate approach, due to the column-wise structure assumed in the model. When inferring  $\alpha$ , we found statistically significant decreases in 5 regions corresponding to the Hippocampus (left), Amygdala (left, right), and the Temporal Pole (T1P, T2P), as shown in Table 1. Full results are plotted in Figure (11) and presented in Section C in the appendix.

In contrast, none of the regions were rejected in the mass-univariate analyses after a BH correction at level .05 (minimal adjusted p-value at .37). For this analysis, we conducted a Welch T-test on each of the off-diagonal elements (after a Fisher transformation), for a total of  $m = 3,655$  tests. Therefore, without constraining the search-space, no significant difference between the groups would be detected (Figure 1). In summary, the application of our method on the TGA data identified significant decays in 5 brain regions, all considered related to the processing of short and long-term memory. By introducing structure, our model had fewer parameters and a reduced number of hypotheses, and was able to detect perturbed regions.

## 7 Discussion

In this paper, we propose a parsimonious model for detecting differences in single variables between correlation-matrix populations. This allows us to control and reduce the number of parameters in the statistical model and avoid the mass loss of power, which results from ad-hoc multiple-comparisons corrections. Our model requires a better description of the cross-dependencies between correlation coefficients, due to both within-subject variability as well as between-subject variability. The parametric framework also shows a substantial gain of power compared to the regularized leading eigenvalue statistic, for which inference is derived using a permutation method. Our model provides estimates

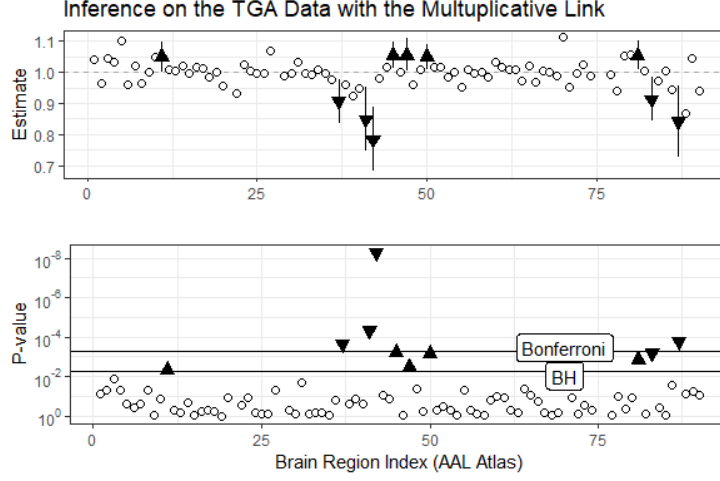


Figure 11: Top: Estimates of  $\alpha$  with FCR-corrected confidence intervals (▼: Significant decay, ▲: significant increase, ○: insignificant). Bottom: The  $\alpha$ 's p-values, in  $\log_{10}$  scale with Bonferroni and BH thresholds.

with useful variance approximations for intermediate-level statistics, as well as powerful statistical tests for partial hypotheses.

Investigating brain connectivity changes in disease states using RS-fMRI represents cases where multiple correlation matrices are compared between groups of subjects. Transient global amnesia represents one such case, where the stark clinical symptoms are not necessarily accompanied by visible brain changes, yet they point to a single lesion in the CA1 part of the hippocampus. Functional MRI can provide important clues as to the origin of the disorder. Previous studies using fMRI (e.g. Peer et al. (2014)) constrained their analyses to the hippocampus and its connectivity, thus potentially missing out on other brain regions involved. Our method, which allows unconstrained data-driven analysis of connectivity disturbances across the brain, revealed that the hippocampus is indeed a core region involved in the disorder. However, additional regions close to the hippocampus (amygdala and temporal pole) were also implicated, indicating a more widespread disruption in the temporal lobe. Specifically, the amygdala disturbance suggests that emotional memory might also be impaired in TGA, opening new avenues for clinical research.

A major challenge of the model is the computational cost of the procedure, mainly the inversion of  $\bar{C}_d$ . In order to allow analyses of larger matrices, this gap must be solved, either with the use of sparse matrices, using the pseudo inverse or introduction of parallelization.

There are natural expansions and generalizations for the model. First, throughout our paper we treated  $\alpha$  as a vector in  $\mathbb{R}^p$ , thus limiting the number of hypothesis tests to the dimension of the correlation matrix in question. How-

ever,  $\alpha$  can be generalized to a matrix of size  $p \times q$  where  $q \geq 1$ . The selection of  $q$  then holds a trade-off between the flexibility of the model and the number of hypotheses to test. Setting a large  $q$  eases the severity of the model assumptions on the data while setting a low  $q$  reduces the number of hypotheses.

Another possible expansion would be the implementation of the model on the partial correlation matrices (Geng et al., 2018; Na et al., 2019). In order to do so, the covariance structure  $\tilde{C}_d$  must be researched and re-evaluated. Lastly, the model should be adjusted for comparing subjects to themselves, as many recent RS-fMRI studies feature intra-subject comparisons (DiNicola et al., 2020; Braga et al., 2020).

In conclusion, we present here a method of discovering differences between groups of correlation matrices. Our findings show that this new methodology can detect localized disturbances in the variables forming the correlation matrices. We believe that this approach can be used to explore existing and new RS-fMRI datasets of different brain disorders, and may be useful in a wide array of additional fields, including neuroscience, economy, and engineering.

## 8 Software and data availability

Our methods, as well as the TGA dataset, are available as an open-source R package [github.com/itamarfaran/corrpops](https://github.com/itamarfaran/corrpops) (2021).

## 9 Appendices

The appendix include proofs for Section 3, additional figures, detailed results for the TGA data, and a description of the sampling algorithms in the simulation.

## Acknowledgments

We thank Yuli Slavutsky, Lee Carlin, Omer Ronen, David Zucker, and Yoav Benjamini for their comments on early versions of this manuscript, and Lihua Lei for valuable discussions.

IF and YB were supported in part by the National Institutes of Health (NIH) R01GM083084, and the German Israeli Foundation. MP was supported by an Eshkol fellowship, an Eva, Luis and Sergio Lamas Fund award, a Fulbright fellowship, and the Zuckerman STEM Leadership Program fellowship. The project was also partially supported by the Center for Interdisciplinary Data Science Research at the Hebrew University.

*Conflict of Interest:* None declared.

## References

- Adrian, D. W., Maitra, R., and Rowe, D. B. (2013). Ricean over gaussian modelling in magnitude fmri analysis added complexity with negligible practical benefits. *Stat*, 2(1):303–316.
- Afyouni, S., Smith, S. M., and Nichols, T. E. (2019). Effective degrees of freedom of the Pearson’s correlation coefficient under autocorrelation. *NeuroImage*, 199:609–625.
- Aitkin, M., Nelson, W., and Reinfurt, K. H. (1968). Tests for correlation matrices. *Biometrika*, 55(2):327–334.
- Baker, J. T., Holmes, A. J., Masters, G. A., Yeo, B. T., Krienen, F., Buckner, R. L., and Öngür, D. (2014). Disruption of cortical association networks in schizophrenia and psychotic bipolar disorder. *JAMA psychiatry*, 71(2):109–118.
- Bartsch, T., Alfke, K., Deuschl, G., and Jansen, O. (2007). Evolution of hippocampal CA-1 diffusion lesions in transient global amnesia. *Annals of Neurology*, 62(5):475–480.
- Bartsch, T., Alfke, K., Stinge, R., Rohr, A., Freitag-Wolf, S., Jansen, O., and Deuschl, G. (2006). Selective affection of hippocampal neurons in patients with transient global amnesia without long-term sequelae. *Brain*, 129(11):2874–2884.
- Benjamini, Y. and Hochberg, Y. (1995). Controlling the false discovery rate: a practical and powerful approach to multiple testing. *Journal of the Royal statistical society: series B (Methodological)*, 57(1):289–300.
- Benjamini, Y. and Yekutieli, D. (2005). False discovery rate-adjusted multiple confidence intervals for selected parameters. *Journal of the American Statistical Association*, 100(469):71–81.
- Biswal, B., Zerrin Yetkin, F., Haughton, V. M., and Hyde, J. S. (1995). Functional connectivity in the motor cortex of resting human brain using echo-planar mri. *Magnetic Resonance in Medicine*, 34(4):537–541.
- Bodwin, K., Zhang, K., and Nobel, A. (2018). A testing based approach to the discovery of differentially correlated variable sets. *The Annals of Applied Statistics*, 12(2):1180.
- Braga, R. M., DiNicola, L. M., Becker, H. C., and Buckner, R. L. (2020). Situating the left-lateralized language network in the broader organization of multiple specialized large-scale distributed networks. *Journal of neurophysiology*, 124(5):1415–1448.

- Brier, M. R., Thomas, J. B., Snyder, A. Z., Benzinger, T. L., Zhang, D., Raichle, M. E., Holtzman, D. M., Morris, J. C., and Ances, B. M. (2012). Loss of intranetwork and internetwork resting state functional connections with Alzheimer’s disease progression. *Journal of Neuroscience*, 32(26):8890–8899.
- Cai, T., Liu, W., and Xia, Y. (2013). Two-sample covariance matrix testing and support recovery in high-dimensional and sparse settings. *Journal of the American Statistical Association*, 108(501):265–277.
- Cai, T. T. (2017). Global testing and large-scale multiple testing for high-dimensional covariance structures. *Annual Review of Statistics and Its Application*, 4:423–446.
- Cai, T. T. and Zhang, A. (2016). Inference for high-dimensional differential correlation matrices. *Journal of multivariate analysis*, 143:107–126.
- DiNicola, L. M., Braga, R. M., and Buckner, R. L. (2020). Parallel distributed networks dissociate episodic and social functions within the individual. *Journal of neurophysiology*, 123(3):1144–1179.
- Dunia, R., Qin, S. J., Edgar, T. F., and McAvoy, T. J. (1996). Identification of faulty sensors using principal component analysis. *AICHE Journal*, 42(10):2797–2812.
- Efron, B. (2008). *Row and column correlations:(are a set of microarrays independent of each other?)*. Division of Biostatistics, Stanford University.
- Efron, B. (2012). *Large-scale inference: empirical Bayes methods for estimation, testing, and prediction*, volume 1. Cambridge University Press.
- Efron, B. and Stein, C. (1981). The jackknife estimate of variance. *The Annals of Statistics*, pages 586–596.
- Faran, I. (2021). corrpops. [github.com/itamarfaran/corrpops](https://github.com/itamarfaran/corrpops).
- Fisher, R. A. (1921). On the probable error of a coefficient of correlation deduced from a small sample. *Metron*, 1:1–32.
- Geng, S., Kolar, M., and Koyejo, O. (2018). Joint nonparametric precision matrix estimation with confounding. *arXiv preprint arXiv:1810.07147*.
- Guo, Y. and Pagnoni, G. (2008). A unified framework for group independent component analysis for multi-subject fmri data. *NeuroImage*, 42(3):1078–1093.
- Hlinka, J., Paluš, M., Vejmelka, M., Mantini, D., and Corbetta, M. (2011). Functional connectivity in resting-state fmri: is linear correlation sufficient? *Neuroimage*, 54(3):2218–2225.
- Jennrich, R. I. (1970). An asymptotic  $\chi^2$  test for the equality of two correlation matrices. *Journal of the American Statistical Association*, 65(330):904–912.

- Lawley, D. (1963). On testing a set of correlation coefficients for equality. *The Annals of Mathematical Statistics*, 34(1):149–151.
- Lee, M. H., Smyser, C. D., and Shimony, J. S. (2013). Resting-state fmri: a review of methods and clinical applications. *American Journal of neuroradiology*, 34(10):1866–1872.
- Liang, K.-Y. and Zeger, S. L. (1986). Longitudinal data analysis using generalized linear models. *Biometrika*, 73(1):13–22.
- Liu, Y., Yu, C., Zhang, X., Liu, J., Duan, Y., Alexander-Bloch, A. F., Liu, B., Jiang, T., and Bullmore, E. (2014). Impaired long distance functional connectivity and weighted network architecture in Alzheimer’s disease. *Cerebral Cortex*, 24(6):1422–1435.
- Locascio, J. J., Jennings, P. J., Moore, C. I., and Corkin, S. (1997). Time series analysis in the time domain and resampling methods for studies of functional magnetic resonance brain imaging. *Human brain mapping*, 5(3):168–193.
- Longin, F. and Solnik, B. (1995). Is the correlation in international equity returns constant: 1960–1990? *Journal of international money and finance*, 14(1):3–26.
- Luo, Q., Misaki, M., Mulyana, B., Wong, C.-K., and Bodurka, J. (2020). Improved autoregressive model for correction of noise serial correlation in fast fmri. *Magnetic resonance in medicine*, 84(3):1293–1305.
- Na, S., Kolar, M., and Koyejo, O. (2019). Estimating differential latent variable graphical models with applications to brain connectivity. *arXiv preprint arXiv:1909.05892*.
- Nel, D. G. (1985). A matrix derivation of the asymptotic covariance matrix of sample correlation coefficients. *Linear algebra and its applications*, 67:137–145.
- Neudecker, H. and Wesselman, A. M. (1990). The asymptotic variance matrix of the sample correlation matrix. *Linear Algebra and its Applications*, 127:589–599.
- Pearson, K. and Filon, L. N. G. (1898). VII. mathematical contributions to the theory of evolution IV. on the probable errors of frequency constants and on the influence of random selection on variation and correlation. *Philosophical Transactions of the Royal Society of London. Series A, Containing Papers of a Mathematical or Physical Character*, (191):229–311.
- Peer, M., Nitzan, M., Goldberg, I., Katz, J., Gomori, J. M., Ben-Hur, T., and Arzy, S. (2014). Reversible functional connectivity disturbances during transient global amnesia. *Annals of neurology*, 75(5):634–643.



- Rabanser, S., Günnemann, S., and Lipton, Z. (2019). Failing loudly: An empirical study of methods for detecting dataset shift. *Advances in Neural Information Processing Systems*, 32:1396–1408.
- Schott, J. R. (2005). *Matrix analysis for statistics*. John Wiley & Sons.
- Schott, J. R. (2007). Testing the equality of correlation matrices when sample correlation matrices are dependent. *Journal of Statistical Planning and Inference*, 137(6):1992–1997.
- Sedlaczek, O., Hirsch, J., Grips, E., Peters, C., Gass, A., Wöhrle, J., and Hennerici, M. (2004). Detection of delayed focal mr changes in the lateral hippocampus in transient global amnesia. *Neurology*, 62(12):2165–2170.
- Sudlow, C., Gallacher, J., Allen, N., Beral, V., Burton, P., Danesh, J., Downey, P., Elliott, P., Green, J., Landray, M., et al. (2015). Uk biobank: an open access resource for identifying the causes of a wide range of complex diseases of middle and old age. *PLoS medicine*, 12(3):e1001779.
- Tzourio-Mazoyer, N., Landeau, B., Papathanassiou, D., Crivello, F., Etard, O., Delcroix, N., Mazoyer, B., and Joliot, M. (2002). Automated anatomical labeling of activations in SPM using a macroscopic anatomical parcellation of the MNI MRI single-subject brain. *Neuroimage*, 15(1):273–289.
- Zheng, S., Cheng, G., Guo, J., Zhu, H., et al. (2019). Test for high-dimensional correlation matrices. *The Annals of Statistics*, 47(5):2887–2921.
- Zhu, L., Lei, J., Devlin, B., and Roeder, K. (2017). Testing high-dimensional covariance matrices, with application to detecting schizophrenia risk genes. *The Annals of Applied Statistics*, 11(3):1810–1831.

## A Proofs from Section 3

### A.1 Conditions for Positive Semi-Definiteness

**Proposition 1.** Define  $\lambda_p \geq 0$  to be the minimal eigenvalue of  $\Theta$ , and  $\alpha_M, \alpha_m$  to be the maximal and minimal values of  $\{|\alpha_1|, \dots, |\alpha_p|\}$ , respectively. For the multiplicative link function  $g$ :

1. For arbitrary  $\alpha$ , if  $\lambda_p \cdot \alpha_m^2 \geq \alpha_M^2 - 1$ , then  $g(\Theta, \alpha)$  is positive semi-definite.
2. Specifically, if  $\alpha_M \leq 1$ , then  $g(\Theta, \alpha)$  is positive semi-definite.

*Proof.* Let  $\Theta \in \mathcal{C}_p$  a correlation matrix, and  $\alpha \in \mathbb{R}^p$ . Consider the multiplicative link function  $g$  in it’s matrix form:

$$g(\Theta, \alpha) = \Theta \circ \alpha \alpha^t + I - D_\alpha^2$$

with  $D_x : \mathbb{R}^p \mapsto \mathbb{M}_p(\mathbb{R})$  defined as

$$[D_x]_{ij} = \begin{cases} x_i & i = j, \\ 0 & \text{otherwise.} \end{cases}$$

We wish to prove that  $x^t g(\Theta, \alpha) x \geq 0 \forall x \in \mathbb{R}^p$ . Write the spectral decomposition of  $\Theta$  as  $\Theta = U \Lambda U^t$ , with  $\lambda_1 \geq \lambda_2 \geq \dots \geq \lambda_p \geq 0$ . Also, recall that:

$$x^t (A \circ B) y = \text{tr}(D_x A D_y B^t) \quad (\text{A.1})$$

$$\max_j a_j \cdot \|x\|^2 \geq x^t D_a x \geq \min_j a_j \cdot \|x\|^2 \forall a \quad (\text{A.2})$$

where A.2 is a result of

$$x^t D_a x = \sum_i a_i x_i^2 \geq \sum_i \min_j a_j \cdot x_i^2 = \min_j a_j \cdot \|x\|^2.$$

Similarly,  $x^t D_a x \leq \max_j a_j \cdot \|x\|^2$ . We wish to find the condition on which  $g(\Theta, \alpha)$  is positive semi-definite,  $x^t g(\Theta, \alpha) x \geq 0$ :

$$\begin{aligned} x^t g(\Theta, \alpha) x &= x^t (\Theta \circ \alpha \alpha^t + I - D_\alpha^2) x \\ &= x^t (\Theta \circ \alpha \alpha^t) x + x^t x - x^t D_\alpha^2 x. \end{aligned}$$

Now, using A.1,

$$\begin{aligned} x^t (\Theta \circ \alpha \alpha^t) x &= \text{tr}(D_x \Theta D_x \alpha \alpha^t) \\ &= \alpha^t D_x \Theta D_x \alpha \\ &= \alpha^t D_x U \Lambda U^t D_x \alpha \end{aligned}$$

And using A.2,

$$\begin{aligned} \alpha^t D_x U \Lambda U^t D_x \alpha &\geq \lambda_p \cdot \alpha^t D_x U U^t D_x \alpha \\ &= \lambda_p \cdot \alpha^t D_x D_x \alpha \\ &= \lambda_p x^t D_\alpha^2 x. \end{aligned}$$

Putting all the above together yields:

$$\begin{aligned} x^t (\Theta \circ \alpha \alpha^t) x + x^t x - x^t D_\alpha^2 x &\geq \lambda_p x^t D_\alpha^2 x + x^t x - x^t D_\alpha^2 x \\ &\geq \lambda_p \alpha_m^2 \|x\|^2 + \|x\|^2 - \alpha_M^2 \|x\|^2 \\ &\propto \lambda_p \alpha_m^2 + 1 - \alpha_M^2 \end{aligned}$$

So for  $x^t g(\Theta, \alpha) x$  to be non-negative, a sufficient condition is:

$$\lambda_p \cdot \alpha_m^2 \geq \alpha_M^2 - 1 \Rightarrow x^t g(\Theta, \alpha) x \geq 0.$$

□

#### Notes:

- If  $0 < |\alpha_j| \leq 1$  for all  $j$ ,  $g(\Theta, \alpha)$  is *always* semi-positive definite as  $\frac{\alpha_M^2 - 1}{\alpha_m^2} \leq 0$  and  $\lambda_p \geq 0$ .
- If  $\max_j \alpha_j > 1$ ,  $\Theta$  must be positive definite ( $\lambda_p > 0$ ).

## A.2 Proof of Identifiability

We provide here more general conditions for identifiability of the multiplicative model, which accommodate cases where  $\alpha_j = 0$  for some of the coordinates of  $\alpha$ . The main difficulty for identifying the multiplicative model are zero values in either  $\Theta$  or  $\alpha$ . For example, when the  $\Theta$  is the identity matrix,  $\alpha$  doesn't affect the model at all. Conversely, if  $\alpha_1, \dots, \alpha_{p-1} = 0$ , the value of  $\alpha_p$  does not affect the model, as all correlation coefficients in  $\Theta \circ \alpha \alpha^t$  would regardless decay to 0.

The main idea is that each non-zero entry in  $\Theta$  gives some information on the two relevant values of  $\alpha$ . We therefore introduce matrices  $A(M)$  that, for a set of indices  $M$ , code all index pairs for which  $\Theta$  is non-zero.

Introducing notation, denote the elementary vector by  $e^{(j)} \in \mathbb{R}^p$  meaning that  $e_i^{(j)} = 1$  if  $i = j$  and  $e_i^{(j)} = 0$  otherwise, and write  $e^{(j,k)} = e^{(j)} + e^{(k)}$ . Then form matrix  $A$  of size  $m \times p$  ( $m = \binom{p}{2}$ ), where the  $\ell$ 'th row is defined as:

$$A_\ell = \mathbf{1} \{ \Theta_{j_\ell k_\ell} \neq 0 \} \cdot e^{(j_\ell, k_\ell)}, \quad \ell = 1, \dots, m. \quad (\text{A.3})$$

Index  $\ell$  iterates over the ordered index pairs  $(j_\ell, k_\ell) = (1, 2), (1, 3), \dots, (p-1, p)$ . For a subset of indices  $M \subseteq \{1, \dots, p\}$ , we define  $A(M)$  to be a filtered version of  $A$ , keeping only those rows where both indices are in  $M$ , and columns which correspond to  $M$ . ( $A(M)$  would therefore have  $\binom{|M|}{2}$  rows and  $|M|$  columns).

**Proposition 2.** *Consider the model (3.1) using the multiplicative link parametrized by  $(\Theta, \alpha)$ , and further assume the coordinates of  $\alpha$  are non-negative. Let  $M_+ = \{j : \alpha_j > 0\}$  be the set of indices where  $\alpha$  is non-zero, and  $M_0 = \{j : \alpha_j = 0\}$  the complementary set. Let  $p_+$  be the size of  $M_+$ . Then the following conditions are sufficient for identifiability:*

1. For every  $j \in M_0$ , exists  $k \in M_+$  so that  $\Theta_{jk} \neq 0$ .
2. The rank of the matrix defined on the non-zero  $\alpha$  coordinates  $A(M_+)$  is  $p_+$ .

*Proof.* Denote  $T(Y) = \{\bar{R}_h, \bar{R}_d\}$ . Our goal is to show that the map  $(\Theta, \alpha) \mapsto E[T(Y)]$  is one-to-one.

Under the multiplicative link,  $E[T(Y)] = \{\Theta, \Theta \circ \alpha \alpha^t\}$ . Therefore  $E[T_1(Y)] = \Theta$  is trivially one-to-one with respect to  $\Theta$ . We are left to prove that for  $\alpha, \beta \in \mathbb{R}^p$ , if  $\Theta \circ \alpha \alpha^t = \Theta \circ \beta \beta^t$  then  $\alpha = \beta$ .

First, we show that the zero-set for vectors  $\alpha$  and  $\beta$  are identical. Consider a non-zero  $\alpha$  coordinate ( $j \in M_+$ ). According to condition (2),  $A(M_+)$  should be of rank  $p_+$ , but only columns corresponding to indices in  $M_+$  are non-zero. Hence, there should be at least one non-zero entry for each column of  $A(M_+)$ . In particular, for  $j \in M_+$  there exists  $k \in M_+$  such that  $\Theta_{jk} \neq 0$ . Therefore  $\Theta_{jk} \alpha_j \alpha_k \neq 0$ . Then  $\Theta_{jk} \beta_j \beta_k \neq 0$  and in particular  $\beta_j \neq 0$ . Next consider a coordinate  $\alpha_j \in M_0$ . From condition (1), there exists coordinate  $k \in M_+$  so that  $\Theta_{jk} \neq 0$ . In particular,  $0 = \alpha_j \alpha_k \Theta_{jk} = \beta_j \beta_k \Theta_{jk}$ .  $\Theta_{jk}, \beta_k \neq 0$ , so  $\beta_j = 0$ .

We are left to show that for  $j \in M_+$ ,  $\alpha_j = \beta_j$ . We have  $p_+$  such parameters, and without loss of generality assume  $M_+ = \{1, \dots, p_+\}$ . For any  $j, k \in M_+$  for

which  $\Theta_{jk} \neq 0$ , we can form the equation

$$|\Theta_{jk}| \cdot \alpha_j \cdot \alpha_k = |\Theta_{jk}| \cdot \beta_j \cdot \beta_k$$

Taking the natural logarithm,

$$\ln |\Theta_{jk}| + \ln \alpha_j + \ln \alpha_k = \ln |\Theta_{jk}| + \ln \beta_j + \ln \beta_k.$$

Denoting  $c_j = \ln \alpha_j - \ln \beta_j$ , we get for each non-zero index in  $\Theta$  an equation  $c_j + c_k = 0$ . Gathering these constraints, we get a linear equation set in  $(c_1, \dots, c_{p_+})$  with a design matrix equivalent to  $A(M_+)$  (A.3):

$$A(M_+) \cdot \begin{bmatrix} c_1 \\ \vdots \\ c_{p_+} \end{bmatrix} = \begin{bmatrix} \vdots \\ 0 \\ \vdots \end{bmatrix}.$$

$\tilde{m} \times p_+ \qquad p_+ \times 1 \qquad \qquad \qquad \tilde{m} \times 1$

Here  $\tilde{m} = \binom{p_+}{2}$ . Given that  $A(M_+)$  is full rank, the only solution is  $(c_1, \dots, c_{p_+}) = \mathbf{0}$ , meaning that  $\ln \alpha_j = \ln \beta_j$  for every  $j \in M_+$ . We conclude  $\alpha_j = \beta_j$  from the monotonicity of the  $\ln$  function.  $\square$

## B Supplementary Figures

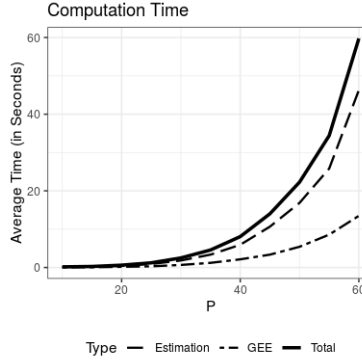


Figure 12: Computation time as a function of  $p$ , showing a complexity of  $O(p^{4.6}) \approx O(m^{2.3})$ . This is the complexity of inverting an  $m \times m$  matrix.

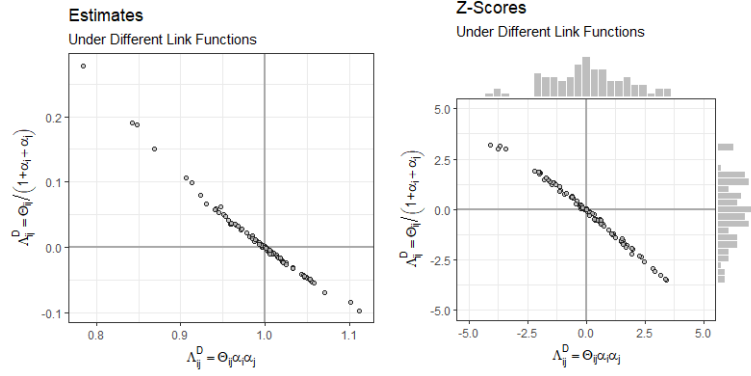


Figure 13: Analysis of the TGA data with different link functions. On the left, quotient link function estimates ( $\Theta_{ij} / (1 + \alpha_i + \alpha_j)$ ) versus multiplicative estimates ( $\Theta_{ij} \alpha_i \alpha_j$ ). On the right, the respective Z-scores. Both links suggest similar results.

## C Full Results on TGA Data

We present all regions with a statistically significant effect identified using the multiplicative link function.

Index	Region	$\tilde{\alpha}$ (s.d)	Z-value	p-value (BH-Adj.)
11	Inferior Frontal Gyrus, Opercular (L) (F3OP)	1.049 (.017)	+2.83	.0397
37	Hippocampus (L) (HIP)	0.907 (.025)	-3.68	.005
41	Amygdala (L) (AMYG)	0.848 (.037)	-4.08	.002
42	Amygdala (R) (AMYG)	0.784 (.037)	-5.84	<.0001
45	Cuneus (L) (Q)	1.054 (.016)	+3.43	.0087
47	Lingual Gyrus (L) (LING)	1.055 (.019)	+2.94	.0316
50	Superior Occipital Lobe (R) (O1)	1.05 (.047)	+3.39	.0087
81	Superior Temporal Gyrus (L) (T1)	1.053 (.016)	+3.19	.0154
83	Temporal Pole: Superior Temporal Gyrus (L) (T1P)	0.913 (.025)	-3.41	.0087
87	Temporal Pole: Middle Temporal Gyrus (L) (T2P)	0.842 (.042)	-3.75	.005

## D Sampling procedures for simulations

---

**Algorithm 1:** Generate Sample Parameters

---

**Input** :  $p, \alpha_{prop}, \alpha_{range}$

**Output:**  $\Theta, \alpha$

1.  $x \leftarrow \mathcal{MN}_{2p \times p}(0, I_{2p}, I_p)$
  2.  $x \leftarrow x^t x$
  3.  $\Theta \leftarrow D_x^{-1/2} \cdot x \cdot D_x^{-1/2}$
  4.  $\alpha_j \leftarrow \text{Unif}(\min(\alpha_{range}), \max(\alpha_{range}))$  for  $j \in \{1, \dots, \alpha_{prop} \cdot p\}$
  5.  $\alpha_j \leftarrow 1$  for  $j \in \{p \cdot \alpha_{prop} + 1, \dots, p\}$
  6. Return  $\Theta, \alpha$
- 

---

**Algorithm 2:** Generate ARMA-Based Covariance Matrix

---

**Input** :  $V \in \mathbb{M}_d(\mathbb{R}), n \in \mathbb{N}, a \in \mathbb{R}^p, m \in \mathbb{R}^q$

**Output:** Symmetric Semi-Positive Matrix

1.  $X \leftarrow \mathcal{MN}_{n \times d}(0, I_n, V)$
  2.  $Y \leftarrow X$
  3. For  $i \in \{1, \dots, n\}$ :
    - (a)  $Y_{i,\cdot} \leftarrow \sum_{j=1}^q m_j X_{i-j,\cdot}$
    - (b)  $Y_{i,\cdot} \leftarrow \sum_{j=1}^p a_j Y_{i-j,\cdot}$
  4.  $W \leftarrow Y^t Y / n$
  5. Return  $W$
-

---

**Algorithm 3:** Generate Samples

---

**Input** :  $\Lambda \in \mathbb{M}_p([-1, 1])$ ,  $n \in \mathbb{N}$ ,  $T \in \mathbb{N}$ ,  $a \in \mathbb{R}^p$ ,  $m \in \mathbb{R}^q$

**Output:** 3-Dimensional Array

1.  $x_j \leftarrow \text{Unif}(\sqrt{10}, 10)$  for  $j \in \{1, \dots, p\}$
  2.  $\Xi \leftarrow D_x \cdot \Lambda \cdot D_x$
  3. For  $i \in \{1, \dots, n\}$ :
    - (a) If  $a, m \neq \emptyset$ :  $W_i \leftarrow \text{Algorithm 2}(\Xi, T, a, m)$   
Else:  $W_i \leftarrow \text{Wishart}_p(\Xi, T)$
    - (b)  $R_i \leftarrow D_{W_i}^{-1/2} \cdot W_i \cdot D_{W_i}^{-1/2}$
  4. Return  $\{R_1, \dots, R_n\}$
-